Adaptive control for a multi-axis hydraulic test rig

A O Gizatullin and **K A Edge***
University of Bath, Bath, UK

The manuscript was received on 31 May 2006 and was accepted after revision for publication on 27 September 2006.

DOI: 10.1243/09596518JSCE314

Abstract: Multi-axis hydraulic rigs are widely used in industrial testing applications but still represent a challenging area for control system design. The current paper considers the control of a six-degrees-of-freedom multi-axis shaking table driven by six hydraulic actuators. The strategy adopted employs adaptive decentralized position control, i.e. each axis has its own adaptive controller. The scheme developed is based on a cascade minimal control synthesis (MCS) approach, which is a class of model reference adaptive control (MRAC). The theoretical background to the controller is presented, together with the results of an experimental study. Performance is compared with three other fixed-gain control schemes. The new adaptive scheme has superior disturbance rejection and command tracking capabilities.

Keywords: multi-axis shaking table, hydraulic actuation, adaptive control, minimal control synthesis

1 INTRODUCTION

Structural testing of specimens, ranging from small components to large complex assemblies, plays a major role in product development. Rigs used for testing large structures are mainly hydraulically actuated. The main advantages of hydraulic actuators over other types of drive are their excellent power density, high precision, and ability to develop large forces. As a consequence, the reproduction of the forces and displacements encountered by the test specimen in service can be achieved with the help of hydraulic actuators arranged in a way that gives a good approximation to realistic operating conditions. Usually the objective of the test is the emulation of a complex loading situation, i.e. when multiple hydraulic actuators are required. Hydraulic test rigs used for this purpose are known as 'multi-axis systems'.

Generally, the purpose of the control system is to achieve high-quality signal tracking, i.e. a close correspondence between the service conditions and those reproduced by the test rig. Classical fixed-gain control schemes may not achieve sufficiently good performance, particularly when applied to multi-axis rigs. The main shortcoming in the control of multi-axis rigs arises from the fact that interactions between the hydraulic drives, and variations in the test specimen parameters during the test, are usually unknown and may significantly degrade the overall control performance. In particular, classical proportional–integral–derivative (PID) controllers may not adequately deal with this problem, and an enhanced control scheme is desirable.

Given the typical nature of the test rig requirements, it was considered necessary to develop a scheme to satisfy the following criteria:

(a) a controller for each axis that either compensates for, or is robust to, interactions from other axes;
(b) an ability to adapt or be insensitive to changes in the specimen characteristics;
(c) close reference position tracking capability.

Publications in the open literature reveal a number of potentially suitable methods for the control of multi-axis hydraulic test rigs. Plummer [**1**], for example, has applied non-linear control to a flight simulation motion system based on a Stewart platform. The author considered acceleration control with non-linear pressure feedback used to linearize the response of the hydraulic actuators and to compensate for the non-linear loading interaction between the actuators. Tsukamoto and Yokota [**2**] studied the performance

* *Corresponding author: Department of Mechanical Engineering, University of Bath, Claverton Down, Bath BA2 7AY, UK. email: K.A.Edge@bath.ac.uk*

of a decentralized two-degrees-of-freedom controller combined with a parallel feed-forward compensator which was applied to a six-link electro-hydraulic manipulator. Performance was compared with that obtained using a decentralized disturbance observer scheme designed using H_∞ theory. Both schemes were shown to achieve good tracking but the two-degrees-of-freedom controller was considered to be easier to design and implement. Significant contributions to control of multi-axis test rigs have been made by De Cuyper and co-workers (e.g. references [**3**] and [**4**]). In reference [**3**] the authors focused on the control of one axis of a four-poster test rig. They proposed an enhancement to an industrial feed-forward controller through the use of a feedback controller designed using H_∞ theory. The experimental results showed that the new scheme resulted in a reduction of tracking error, over a frequency range of 2 to 25 Hz, when compared with the feed-forward controller acting alone. A related study, concerned with the control of a two-axis durability suspension test rig, is reported in reference [**4**]. Once again the control scheme comprised a feed-forward path (designed iteratively off-line) enhanced with a feedback controller designed using an H_∞ methodology. It was shown that with the enhanced scheme, for the same level of tracking accuracy, the number of iterations required to design the feed-forward controller was reduced from 7 to 3, leading to a significant saving in time.

Adaptive control schemes for multi-axis systems have also received serious attention by various researchers. Edge and Gomes de Almeida [**5**], for example, studied the application of model reference adaptive control to a two-axis hydraulically actuated manipulator. Their scheme adopted decentralized control and was designed using variable structure control theory. It was shown experimentally that very good model-following and axis decoupling could be achieved over a wide range of operating conditions. Gomez [**6**] successfully applied an (adaptive) minimal control synthesis (MCS) scheme to control the University of Bristol shaking table (which is used for earthquake studies of buildings). The author developed a decentralized MCS controller combined with a PID compensator. These and other research studies on adaptive schemes have demonstrated the potential for controlling complex hydraulically actuated multi-axis machines in which the goal is to achieve consistent dynamic performance in the presence of non-linearities, disturbances, and varying loads. The motivation for the work reported in the current paper was the achievement of such characteristics in combination with high-fidelity input tracking. It was decided to base the design of the adaptive controller on the MCS principle, because of the relative ease of controller parameter selection and controller implementation. Owing to the nature of the load acting on the hydraulic actuators, a cascade control scheme has been adopted in which the inner control loop relates cylinder piston velocity to the servo-valve input signal. Additionally, a feed-forward inverse reference model arrangement has been introduced in order to meet a command signal tracking requirement.

The present paper is organized as follows: section 2 describes the experimental test facility used for testing of the adaptive controller; section 3 provides insight into the adaptive control concept design; in section 4 an experimental validation of the control concept is presented and its performance is compared with three other fixed-gain schemes; finally, conclusions are drawn in section 5.

2 EXPERIMENTAL TEST FACILITY

2.1 Multi-axis shaking table layout

A multi-axis shaking table (MAST) test rig is designed to recreate spatial motion of the table in three dimensions with the test specimen mounted upon it. This type of test rig is commonly used for durability testing, for example performance, squeak, and rattle evaluation of an automobile. The MAST at the University of Bath Laboratory was manufactured and supplied by Instron Structural Testing Systems (IST®) with an industrial Labtronic™ 8800 Digital Controller. The rig is shown in Fig. 1 and the specification of the MAST is given in Table 1.

The MAST rig has three vertical hydraulic cylinders producing vertical, pitch, and roll motion; two horizontal lateral cylinders for lateral and yaw motion; and, finally, a horizontal longitudinal cylinder used for longitudinal motion of the platform. Each of the horizontal cylinders is mounted in a pedestal and transmits motion via pushrods connected between the cylinder rod and the table by a universal joint. The vertical cylinders are mounted on an anchored base and attached to the table by two universal joints. The stall force of each cylinder is 25 kN except for the horizontal longitudinal cylinder, which is 33 kN (because it acts alone and hence is required to take a higher load than the other cylinders). Each cylinder is driven by a fast-acting MOOG™ servo-valve with a 65 l/min rated flow capacity. The hydraulic cylinders, manufactured by Hydropuls™, are double ended and double acting with improved dynamic characteristics over general

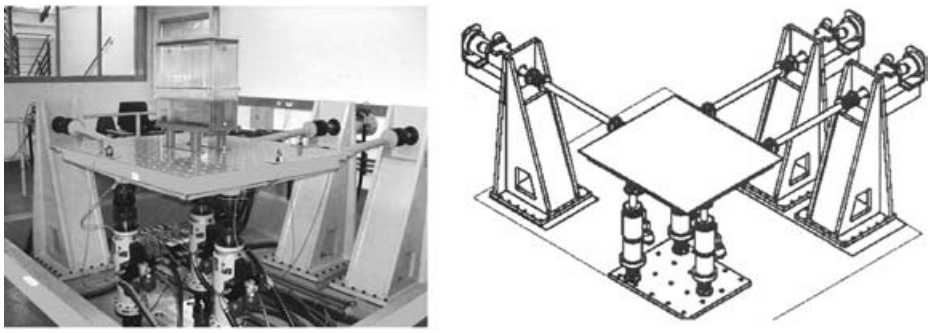

Fig. 1 MAST at the University of Bath Laboratory

Table 1 Specification of the MAST

Longitudina1 actuator load rating	33 kN
Other actuators load rating	25 kN
Actuator stroke	$\pm$75 mm
Servo-valve rated flow Q_{Rated} (70 bar pressure drop ΔP_{Rated})	65 l/min
Peak velocity (no payload) – vertical	1.5 m/s
Peak velocity (no payload) – lateral	1.25 m/s
Peak velocity (no payload) – longitudinal	1 m/s
Peak acceleration (max payload 450 kg) – vertical	8 g
Peak acceleration (max payload 450 kg) – lateral	5 g
Peak acceleration (max payload 450 kg) – longitudinal	3 g
Oil supply pressure	280 bar
Oil supply flow	165 l/min

industrial cylinders. Low levels of friction are achieved by mounting the piston rod in hydrostatic bearings.

The six-degrees-of-freedom motion of the table, i.e. the position of the table mass centre in space, together with the pitch, yaw, and roll angles, is geometrically related to the corresponding position of each of the six actuators. From the known geometrical coupling of the legs to the table, the required position of the mass centre of the table and the table's angular position are determined by evaluating the corresponding distribution of the command signals between the actuators using an inverse kinematical model.

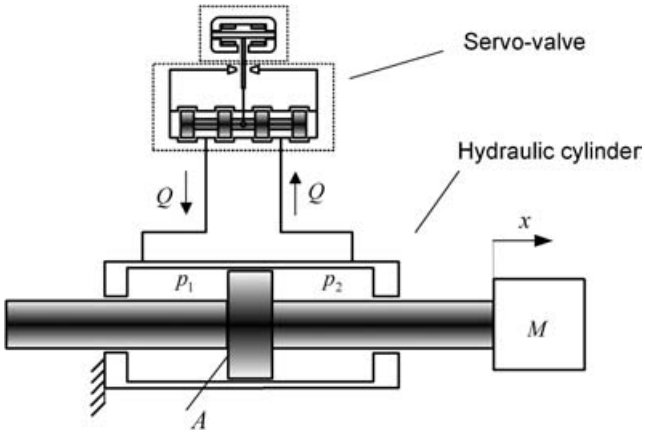

Fig. 2 Schematic diagram of a hydraulic actuator

2.2 Linear model of hydraulic actuator dynamics

The derivation of the hydraulic actuator dynamics is based on the commonly adopted assumptions that the servo-valve dynamics are sufficiently fast to be neglected, the trapped volume in both actuator ends is equal and invariable, piston friction is negligible, cylinder support stiffness and rod stiffness are infinite, and cross-piston leakage and manifold pressure losses are negligible.

As shown in Fig. 2, a hydraulic actuator consists of a servo-valve supplying flow to a hydraulic cylinder with the load acting on the cylinder piston rod. The servo-valve is an electro-hydraulic flow control device. The flowrate has a non-linear relationship with the servo-valve spool displacement and pressure in the hydraulic cylinder, which, in turn, is governed by the load acting on the cylinder piston rod. This relationship represents the main non-linearity of the hydraulic servo-system and, for the case of a symmetrical double-acting cylinder with negligible friction, is given by

$$Q = K_{\text{V}} x_{\text{SV}} \sqrt{\frac{|p_{\text{SYS}} - p_{\text{L}}|}{2}} \operatorname{sign}(p_{\text{SYS}} - p_{\text{L}}) \tag{1}$$

where

K_{V} is flow gain
x_{SV} is spool displacement

p_{SYS} is system pressure $[p_S - p_R]$
p_L is load pressure $[p_1 - p_2]$.

The spool displacement is non-dimensionalized and can vary within the limits of $(-1, 1)$. The flow gain K_V incorporates factors relating to the geometry of spool bushing metering orifices, flow discharge coefficient dependence on Reynolds number, and fluid density. The flow gain K_V can be evaluated from the rated flow Q_{Rated} and the corresponding pressure drop ΔP_{Rated} supplied by the manufacturer. Here the servo-valve flow gain is defined as

$$K_V = \frac{Q_{Rated}}{\sqrt{\Delta P_{Rated}/2}} \tag{2}$$

From a detailed analysis, the bandwidth of the servo-valve was found to be much greater than the bandwidth of the hydraulic cylinder; hence the dynamics of the servo-valve are assumed to be sufficiently fast to be neglected. Therefore, the servo-valve position x_{SV} is equal to the valve input signal u when represented in non-dimensional form, i.e.

$$x_{SV} = u \tag{3}$$

In order to express the system dynamics in the form of a transfer function, it is necessary to linearize the system equations. Linearization of the flow–pressure relationship (equation (1)) is determined by the specific operating condition of the system and is described by the value of the servo-valve spool displacement x_{SVO} and the load pressure p_{LO}. Selection of these values is derived from a known nominal service load acting on the actuator. The linearized representation of the flow–pressure relationship is

$$Q = K_{QX} x_{SV} - K_{QP} p_L \tag{4}$$

where

K_{QX} is valve flow-spool displacement coefficient
K_{QP} is valve flow-pressure coefficient

and

$$K_{QX} = \left|\frac{\partial Q}{\partial x_{SV}}\right|_{\substack{X_{SV}=X_{SVO}\\ P_L=P_{LO}}} = K_V\sqrt{\frac{|p_{SYS} - p_{LO}|}{2}} \tag{5}$$

$$K_{QP} = \left|\frac{\partial Q}{\partial p_{SV}}\right|_{\substack{X_{SV}=X_{SVO}\\ P_L=P_{LO}}} = \frac{K_V x_{SVO}}{2\sqrt{2(|p_{SYS} - p_{LO}|)}} \tag{6}$$

The flowrate from the servo-valve matches the flow required to move the actuator piston plus a compensating flow term that accounts for the compressibility of the trapped oil volume, thus

$$Q = A\dot{x} + \frac{V_o}{2B}\dot{p}_L \tag{7}$$

where

A is effective area of the cylinder
B is bulk modulus
V_o is trapped volume of oil in the chambers of the cylinder and connected piping.

With negligible friction the load on the piston rod is purely inertial and the piston motion is described by

$$M\ddot{x} = Ap_L \tag{8}$$

From equations (3), (4), (7), and (8) a transfer function $W_{HA}(s)$ for the hydraulic drive can be derived

$$W_{HA}(s) = \frac{K_P\omega_P^2}{(s^2 + 2\xi_P\omega_P s + \omega_P^2)s} \tag{9}$$

Where the plant gain K_P is

$$K_P = \frac{K_{QX}}{A} \tag{10}$$

The natural frequency ω_P of the actuator (or oil column resonance frequency) is

$$\omega_P = \sqrt{\frac{2A^2B}{MV_o}} \tag{11}$$

And the damping ratio ξ_P is given by

$$\xi_P = \frac{1}{2}\left(\frac{K_{QP}M}{A^2}\right)\sqrt{\frac{2A^2B}{MV_o}} \tag{12}$$

A block diagram for the linearized hydraulic actuator dynamics is shown in Fig. 3. It follows from the linearization procedure that the actuator transfer function can be represented by a second-order transfer function between the servo-valve drive signal and the cylinder velocity (corresponding to a velocity cascade) and a pure integrator.

The coefficients K_P, ξ_P are functions of the linearization coefficients K_{QX} and K_{QP} given by equations (5), (6) and hence depend on the current operating (linearization) point. The natural frequency

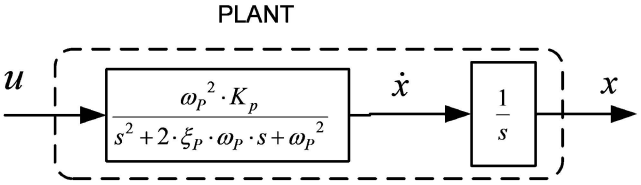

Fig. 3 Block diagram of a hydraulic actuator

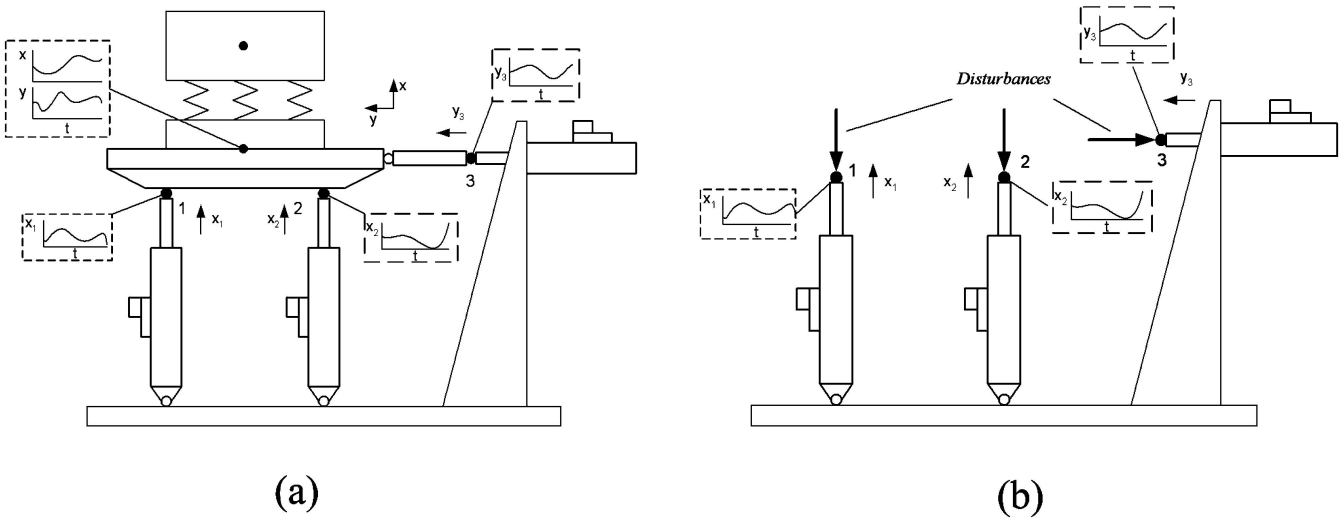

Fig. 4 Decentralized control scheme of the MAST

ω_P is a function of the bulk modulus B and the trapped oil volume V_o and can be viewed as being time-dependent since the trapped volume varies during operation and the oil bulk modulus has a complex dependence on the physical condition of the oil and does not hold a unique value. Therefore, over the operating cycle, the parameters of the linear model are time-varying owing to the non-linearity of the plant.

3 ADAPTIVE CONTROLLER DESIGN

In this section a concept for an adaptive control scheme is presented. The decoupled control principle, which is the foundation of the chosen strategy, is presented in section 3.1. This is followed by a description of the adaptive controller concept that has been adopted, and its application, in sections 3.2 and 3.3 respectively.

3.1 Decoupled controller solution

An example of the application of a decentralized type of control scheme to the MAST is presented in Fig. 4. Suppose that the purpose of the MAST is to follow a target motion at the mass centre of the table when a sprung specimen is mounted on top. Further suppose that this can be achieved by appropriate displacement of three cylinders: two vertical and one horizontal (see Fig. 4(a)). The difficulty in control arises from the mass of the table and specimen inertia resulting in varying forces acting on each cylinder. In addition there may be resonance modes of the specimen, resulting in additional loads on the cylinders. With a decentralized controller each axis is controlled independently, with interactions between axes (originating from the inertia and resonance-induced forces of the specimen) being treated as disturbances (see Fig. 4(b)).

3.2 Control concept

MCS, shown in block diagram form in Fig. 5, was introduced by Stoten and co-researchers [**7**–**9**] and is an extension of model reference adaptive control (MRAC). The design of the MCS algorithm has the advantage that it does not require a thorough synthesis of the controlled plant and controller. One of the extensions to the standard MCS scheme, which is used in the current paper, is MCS with integral action [**10**] (MCSIA), which enhances the adaptation performance of the standard MCS controller.

The governing equations of the MCSIA control algorithm are given below (the equations for the adaptive gains (14), (15), and (16) included a *sign*

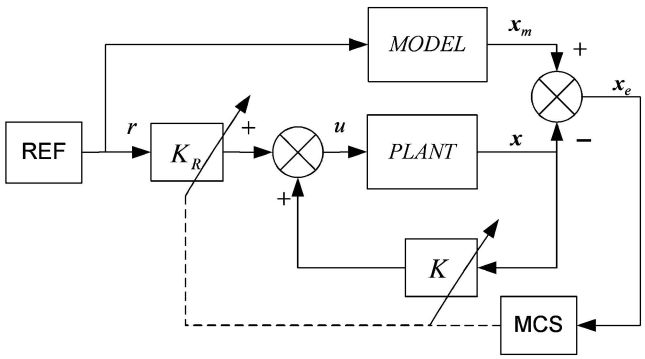

Fig. 5 Minimal controller synthesis block diagram

function in order to remove amplitude sensitivity of the gains)

$$u(t) = \boldsymbol{K}(t)\boldsymbol{x}(t) + K_{\mathrm{R}}(t)r(t) + K_i x_i(t) \tag{13}$$

$$\boldsymbol{K}(t) = \int_0^t \alpha y_{\mathrm{e}}(\tau)\,\mathrm{sign}(x^T(\tau))\,\mathrm{d}\tau + \beta y_{\mathrm{e}}(t)\,\mathrm{sign}(x^T(t)) \tag{14}$$

$$K_R(t) = \int_0^t \alpha y_{\mathrm{e}}(\tau)\,\mathrm{sign}\,(r(\tau))\,\mathrm{d}\tau + \beta y_{\mathrm{e}}(t)\,\mathrm{sign}(r(t)) \tag{15}$$

$$K_i(t) = \int_0^t \alpha y_{\mathrm{e}}(\tau)\,\mathrm{sign}(x_i^{\mathrm{T}}(\tau))\,\mathrm{d}\tau + \beta y_{\mathrm{e}}(t)\,\mathrm{sign}(x_i^{\mathrm{T}}(t)) \tag{16}$$

The scalar error $y_{\mathrm{e}}(t)$ is the product of the state error vector $\boldsymbol{x}_{\mathrm{e}}(t)$ (which is the difference between model and plant state vectors) and the linear compensator vector $\boldsymbol{C}_{\mathrm{e}}$.

$$y_{\mathrm{e}} = \boldsymbol{C}_{\mathrm{e}}^{\mathrm{T}}\boldsymbol{x}_{\mathrm{e}} \tag{17}$$

The integral state error $x_i(t)$ is

$$x_i(t) = \int_0^t (r(\tau) - x(\tau))\,\mathrm{d}\tau \tag{18}$$

The parameters to be assigned by the designer are those relating to the reference model, the compensator vector, and the adaptive weights, α and β.

It follows from Fig. 5 that the plant has a full state adaptive feedback and a forward adaptive gain. Adaptive gains are tuned by the MCS adaptive mechanism given by equations (14), (15), and (16). Adaptation aims to achieve a situation where the dynamics of the plant, closed by the adaptive feedback loop and in combination with the adaptive forward term, match those defined by the model transfer function. Such a controller should exhibit robustness to disturbances arising from the plant parameter variations, non-linearities of the plant, and load variations.

Velocity MCS (denoted hereafter as vMCS) is an extension of the MCS and MCSIA controllers, which is introduced here and which is applied to control the velocity cascade of the hydraulic plant. The velocity cascade is the second-order transfer function of the linearized plant shown in Fig. 3. Since vMCS specifies the behaviour solely of the plant cascade, a conventional fixed-gain controller (such as a PID scheme) must be introduced in order to control the position of the piston.

The block diagram of the vMCS controller is shown in Fig. 6. The adaptive scheme controls the velocity cascade of the plant. The integrator after the plant cascade corresponds to the pure physical integral action of the actuator as described in section 2.2. Strictly, the number of feedback signals required to construct an adaptive controller should be equal to the order of the cascade transfer function. In this case the linearized plant cascade is of order two; therefore, two states are necessary for the feedback, namely velocity and acceleration. In total the adaptive controller requires four adaptive gains, i.e. two adaptive gains in the feedback (velocity and

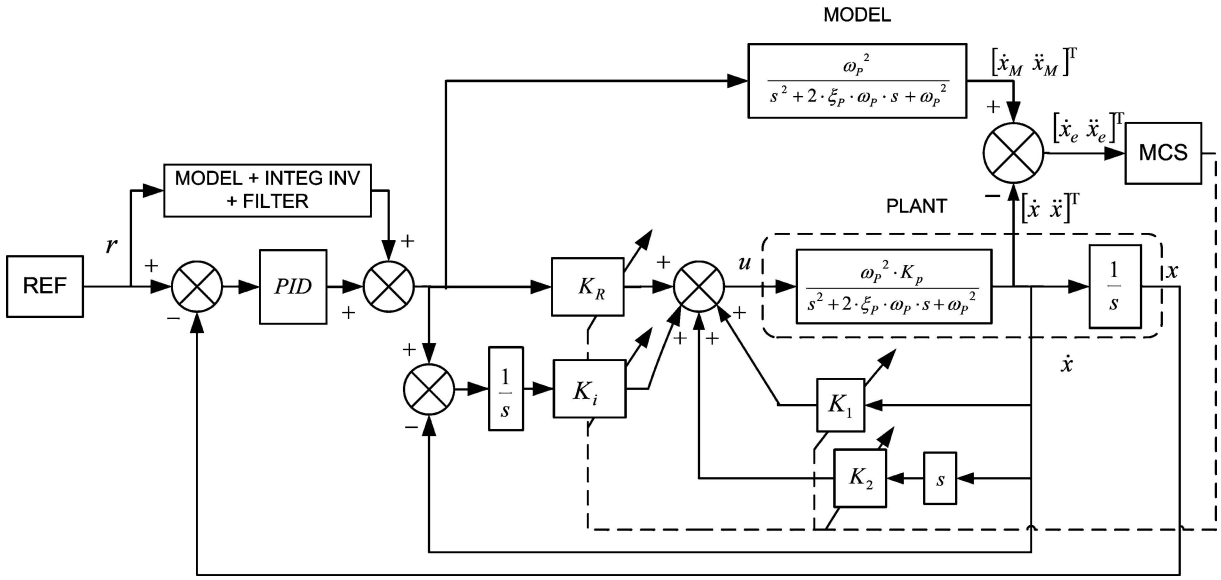

Fig. 6 Velocity MCS (vMCS)

acceleration), one forward adaptive gain, and an additional integral adaptive gain. Provided model following can be achieved, the hydraulic actuator with the adaptively controlled velocity cascade can be represented by the block diagram given in Fig. 7.

Once the vMCS controller has been applied to the plant cascade the overall dynamics of the plant under position feedback control are known. Performance can be further enhanced by adopting a two-degrees-of-freedom controller arrangement, i.e. to introduce an approximation to the inverse of the model of the controlled plant as a feed-forward block, with the reference signal as its input and with the output added to the PID control signal, as shown in Fig. 8. This two-degrees-of-freedom adaptive controller is termed here as IMvMCS (inverse model velocity MCS). Arranged in this way, the controller aims to cancel out the plant dynamics leaving, ideally, a unity transfer function. In order to implement this controller, acceleration and velocity signals are required by vMCS supplemented by the position signal used by a conventional PID controller. A similar approach, but without the adaptive elements, has been reported by Hessburg and Kranz [**11**]. They applied the technique in combination with a three-variable feedback controller which was introduced to ensure the stability of the system. This two-degrees-of-freedom controller used all known information about the desired test waveforms, actuation system, and specimen properties, and it was assumed that all *a priori* knowledge of the system parameters was correct.

Adaptation dynamics of this new controller are not considered in the current paper. Generally, it is assumed that the input signal is persistently exciting or is sufficiently 'rich' to achieve model following. This aspect of adaptive systems has been analysed by, *inter alios*, Bitmead [**12**]. Adaptation behaviour can be complex, with the possibility that, in some circumstances, the system may exhibit highly nonlinear and chaotic dynamics [**13**]. For the studies reported in the present paper it is assumed that the input signal possesses the property of being persistently exciting, in which case the efficacy of the feed-forward inverse model arrangement in the IMvMCS scheme holds.

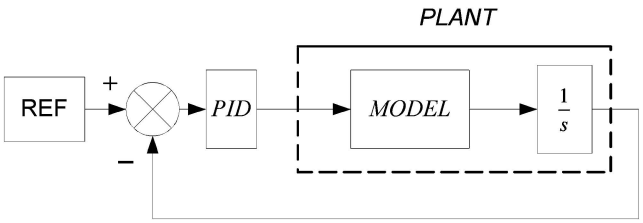

Fig. 7 Block diagram for a successfully-controlled adaptive velocity cascade

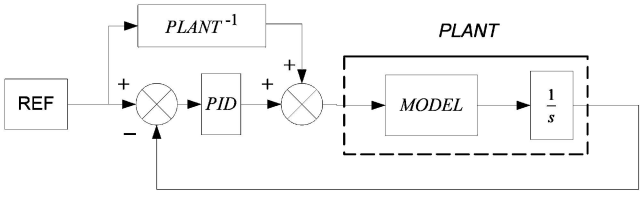

Fig. 8 Block diagram for the inverse model feed-forward scheme

3.3 Implementation of the controller

Strictly, in order to implement the adaptive controller, measurements of the displacement, velocity, and acceleration are required. The test rig cylinder had a displacement sensor and accelerometer attached at the end of the piston rod. The velocity of the cylinder was obtained by passing the raw displacement and acceleration signals via a set of filters that aimed to provide a zero phase lag filtered velocity signal. This approach, sometimes referred to as 'fusion of kinetic data using composite filters', has been described in detail by Stoten [**14**]. The principle is as follows. A velocity estimate is obtained as the sum of the measured position and acceleration signals that have been passed through low-pass and high-pass filters respectively. The parameters for the composite filter are chosen to ensure that noise content is substantially attenuated and, within the overall operational bandwidth of the system, valuable signal information remains. For this study the cut-off frequency was chosen to be 20 rad/s. However, owing to the cylinder mount compliance the measured acceleration of the piston rod included an undesired effect arising from the mount motion. In order to obtain the cylinder piston rod *relative* acceleration, an additional accelerometer was attached to the cylinder mount and the difference between the two accelerometer signals was determined. Thus, in order to estimate velocity, both the relative acceleration and the measured position of the cylinder piston rod were used.

The accelerometer installed at the piston rod was also found to pick up unwanted information induced by the pressure pulsations transmitted from the hydraulic pump. This 'noise' component of the acceleration signal was found to create system instability when used as an adaptive feedback signal. Application of the composite filter to obtain a filtered acceleration signal from displacement and acceleration was unsuccessful because the high-pass filter for acceleration was not sufficiently effective in

attenuating noise. As a result, it was not possible to include acceleration as a feedback signal. Although simulation studies provided evidence that the absence of the acceleration feedback results in some loss of performance, it was still possible to design an effective scheme, as discussed below.

The inverse feed-forward block shown in Fig. 8 was made realizable by combining it with a filter of the same order as the inverse plant model but with a higher bandwidth. The bandwidth was chosen such that the desired bandwidth of the system was achievable without parasitic effects on the amplitude and phase characteristics of the filter. In order to preserve the integrity of the controlled loop a similar filter was introduced to act on the command signal. Thus, the aim of the controller was to track a filtered version of the command signal. Figure 9 provides a detailed block diagram of the adaptive controller scheme, and Fig. 10 shows the arrangement for the implementation of the controller. It should be noted from Fig. 9 that the scheme incorporates a conventional fixed-gain PIDL block which is, in fact, the standard commercial controller for the MAST (Labtronic™ 8800 Digital PIDL Controller). The PIDL is a classical PID controller combined with an additional first-order lag transfer function. The lag term is introduced to maximize the amplitude margin of the open-loop frequency response of the controller.

For the adaptive vMCS element of the controller, the following parameters need to be defined: a second-order reference model (defined by K_M, ω_M, and ξ_M), values for the coefficients of the $\boldsymbol{C}_e$ vector, and, finally, the adaptive weights α and β. Owing to the use of the inverse model, the reference model was selected in order to achieve faster and better adaptation. The choice of the model parameters defines the adaptation rate and bandwidth of the adaptively controlled system. Selection of $\boldsymbol{C}_e$ followed

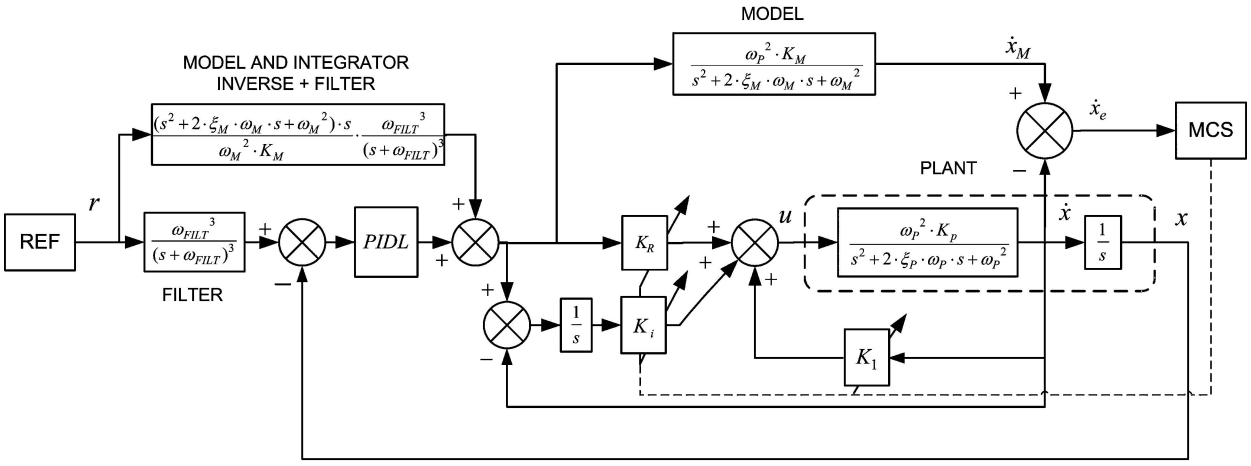

Fig. 9 Block diagram of the inverse model velocity MCS (IMvMCS)

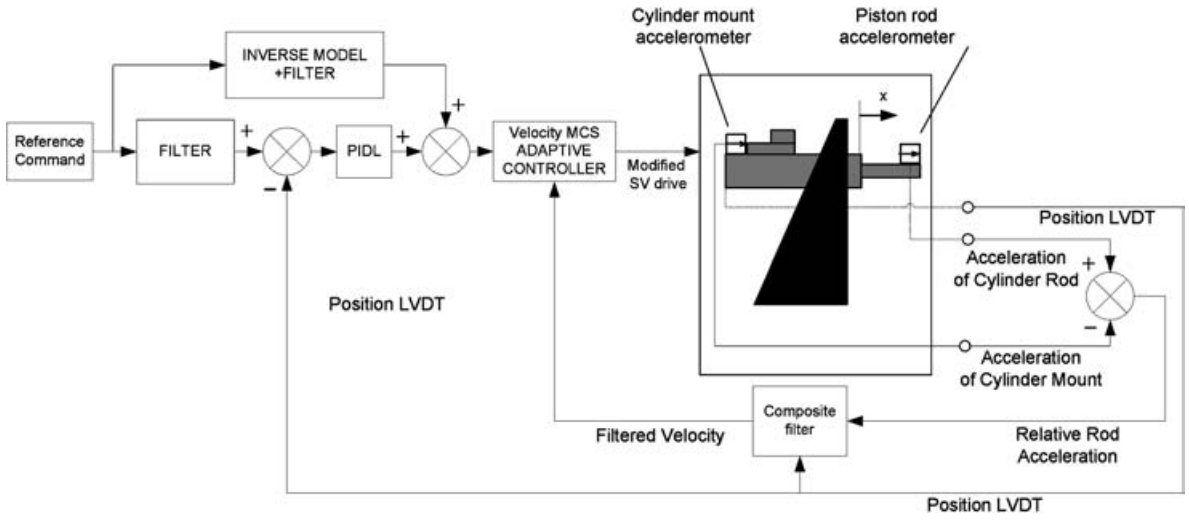

Fig. 10 Arrangements for the implementation of the adaptive controller

the guidance of Gomez [**6**]. In this particular implementation, because only velocity feedback is used, $\boldsymbol{C}_e$ is a scalar and a value of unity is appropriate. The values for the adaptation weights α and β were chosen empirically, while keeping the ratio α/β equal to 10 according to the guidance given by Stoten [**7**]. The analysis of the adaptation rate is outside the scope of the present paper; however, it was observed experimentally that better adaptation occurs if the selected model has a bandwidth that is roughly the same as, or slightly larger than (say by 30 per cent), the natural frequency of the plant cascade.

There are a number of factors that influence the operational bandwidth of the controlled system. The first issue is the saturation of the valve. For higher frequency demands the command signal from the inverse model will reach sufficiently large values to cause the valve to saturate, leading to an integrator wind-up problem. This can be solved by locking the values of adaptive gains, and hence stopping the adaptation, at the point when the servo-valve is saturated. Second, the inverse model requires a filter with a bandwidth that is limited by the nature of the command signal. If the signal is discontinuous then a filter of higher bandwidth will give undesired spikes, owing to the 'infinite' value of the demanded acceleration associated with the discontinuity in the command signal. Third, for certain command signals, unmodelled high-frequency dynamics of the system may be excited, introducing undesired disturbances which the adaptive controller was not designed to accommodate. Finally, the exclusion of the acceleration signal introduces a limitation on the bandwidth of the tracking capability of the adaptive controller for sine-wave inputs. This was found to be 15 Hz. (The 15 Hz tracking capability was established experimentally by means of providing a series of discrete sine-wave command inputs over a frequency range from 1 to 20 Hz; at frequencies above 15 Hz the adaptive controller lost tracking capability and exhibited a drift-and-burst phenomenon [**15**].)

4 EXPERIMENTAL STUDIES

The experimental studies were aimed at examining the disturbance rejection properties of the new controller and assessing its performance in comparison with fixed-gain control strategies. The controllers used for comparison purposes were the industry-standard PIDL controller and two other schemes which were variants of the fixed-gain two-degrees-of-freedom controller design concept described in section 3.2.

The disturbance rejection properties of the controller were tested on the MAST horizontal axis Y1 as shown in Fig. 11. The reference command to the Y1 axis was 'pink' noise with a 20 Hz bandwidth. Axis Y2 was used as the disturbance source. The motion of the Y2 axis was an 8 Hz sine-wave with an amplitude of 10 mm, which was found to create sufficient interaction to be noticeable when using the conventional PIDL controller. The interaction acting on axis Y1 originated from the total inertia of the table and vertical legs. To compare the effect of the disturbance rejection capabilities of the various control schemes, tests were run for the disturbed and undisturbed cases. In the undisturbed case the Y2 axis was stationary.

In order to design the comparative controllers a plant transfer function estimate was obtained from a plant identification procedure. A random signal of 1–20 Hz bandwidth was fed to the input of the industry-standard PIDL position control loop, and the corresponding servo-valve drive signal and actuator velocity were measured. The signals were processed in the MATLAB Identification Toolbox and a second-order transfer function approximation was matched to the measured data with 91.4 per cent fit. The fitness of the model was estimated from equation (19) in which Y and $\hat{Y}$ are the measured and model responses respectively

$$\text{FIT} = \left(1 - \frac{\| Y - \hat{Y} \|}{\| Y - \text{mean}(Y) \|}\right) 100 \tag{19}$$

The estimated plant cascade transfer function parameters were as follows

$\tilde{K}_P = 1.85$	estimated plant gain
$\tilde{\omega}_P = 112$ rad/s	estimated natural frequency
$\tilde{\xi}_P = 0.55$	estimated damping ratio

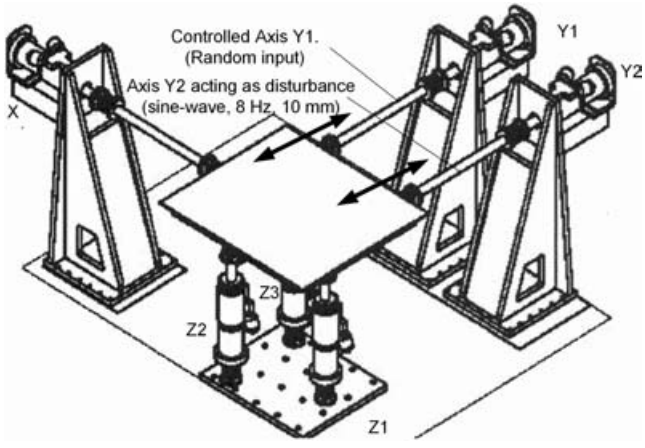

Fig. 11 Table axes, as used for the experimental studies

To provide a benchmark, the PIDL controller was initially tuned to achieve as fast a response as possible, without exceeding a 30 per cent overshoot, when presented with a 1 mm square wave. Because the PIDL controller could not match the adaptive controller, owing to its simplicity and inability to follow the command trajectory (as discussed below), two additional and more advanced comparative controllers were designed for the task. These comparative controllers were chosen with a nominal inverse plant transfer function in the feed-forward path. This type of controller relies on the assumption that the plant is linear and the transfer function of the plant is known.

The first fixed-gain scheme (denoted hereafter as 'case 1') is shown in Fig. 12. Here the feed-forward inverse block was selected on the basis of the estimated plant transfer function. Such an arrangement is similar to the adaptive controller shown in Fig. 8 with the absence of the adaptive part. As in the adaptive case, filters were used for the plant inverse block (in order to make the inverse model physically realizable) and likewise for the reference command signal in order to maintain the integrity of the control loop. The parameters of the model were identical with the estimated plant parameters; model gain, natural frequency, and damping ratio were $K_{M1} = \tilde{K}_P = 1.85$, $\omega_{M1} = \tilde{\omega}_P = 112$ r/s, and $\xi_{M1} = \tilde{\xi}_P = 0.55$ respectively.

The second type of fixed-gain scheme (denoted hereafter as 'case 2') is shown in Fig. 13. The plant had fixed-gain velocity and acceleration feedback paths, together with a fixed-gain forward path. Such an arrangement acts as a pole placement controller (in the figure the pole-placement part of the controller is identified by the bold dotted line). Feedback and forward gains of the controller were calculated from the parameters associated with the desired dynamics of the plant and also its estimated parameters. The desired dynamics of the pole-placement control were chosen to create a system that was faster and more damped. This was achieved by setting the required natural frequency for the target of the pole-placement control to be 30 per cent larger than that estimated. The new values for the model gain, natural frequency, and damping ratio were $K_{M2} = 1.85$, $\omega_{M2} = 145$ r/s, and $\xi_{M2} = 0.9$ respectively. For the given model, the gains were $K_R = 1.69$, $K_1 = -0.373$, and $K_2 = -0.006$ respectively.

The parameters of the adaptive IMvMCS controller were as follows. The natural frequency was chosen to be 30 per cent larger than that estimated for the plant; this was also selected for controller 'case 2'. Therefore the parameters of the model

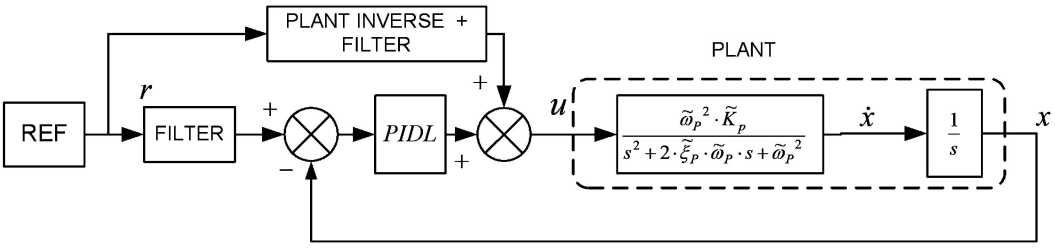

Fig. 12 Block diagram for comparative controller 'case 1'

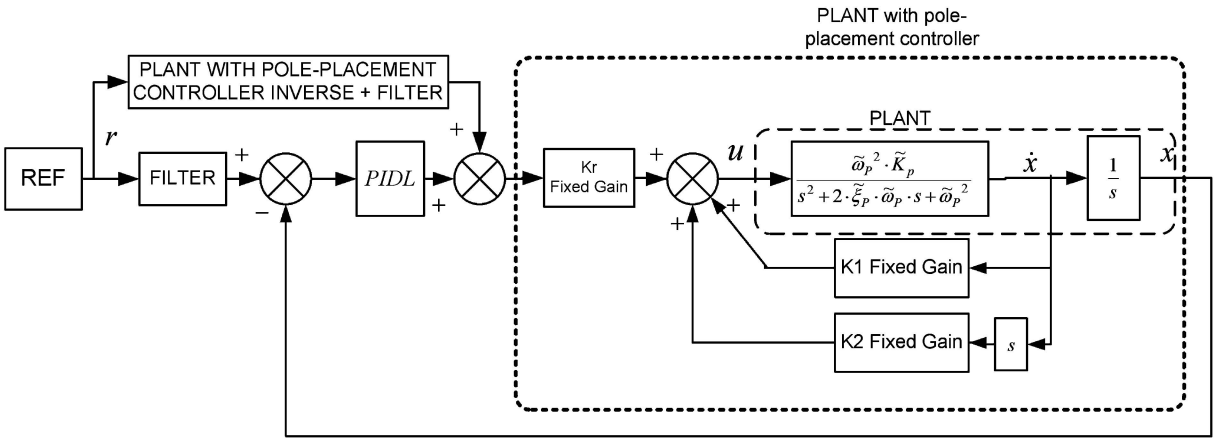

Fig. 13 Block diagram for comparative controller 'case 2'

were: the normalized plant gain, $K_M = 1/1.72 = 0.581$ (normalized on the basis of the maximum unloaded piston velocity, which was found to be equal to 1.72 m/s); model natural frequency, $\omega_M = 145$ r/s; model damping ratio, $\xi_M = 0.9$; and adaptive weights α and β were 0.3 and 0.03 respectively. The initial value for the adaptive gain K_R was unity. This was done in order to avoid the plant response dropping to zero over the adaptation transient period. The other two adaptive gains K_1 and K_i were set to zero at the start of adaptation.

The performance of the adaptive scheme is shown in Fig. 14. This figure illustrates the transient behaviour following the switch from conventional PIDL control to adaptive control. Figures 14(a) and (b) display the tracking of the filtered reference signal (shown as thin line) by the actuator position (shown as bold line) and the position tracking error. Figure 14(c) shows the behaviour of the forward (K_R), velocity feedback (K_1), and integral (K_i) adaptive gains. The start of the adaptation is indicated by the step change of gain K_R at 2.8 s. It can be clearly seen that over a period of approximately 5 s the maximum position tracking error reduces from a peak level of 4 mm to 1 mm. This is also reflected in Fig. 14(a) where the position of the cylinder can be seen progressively to track the filtered reference signal more faithfully.

A comparative analysis of the disturbance rejection properties of the PIDL and adaptive controller schemes is shown in Fig. 15. The comparison was done on the basis of the difference between the cylinder displacement deviation with and without the presence of the disturbance. Figures 15(a) and (c) indicate, on an enlarged time scale, the cylinder position under PIDL and adaptive control for both the disturbed and undisturbed cases, plotted against similar time intervals for the same random command input. Figures 15(b) and (d) show the position tracking error for the disturbed and undisturbed

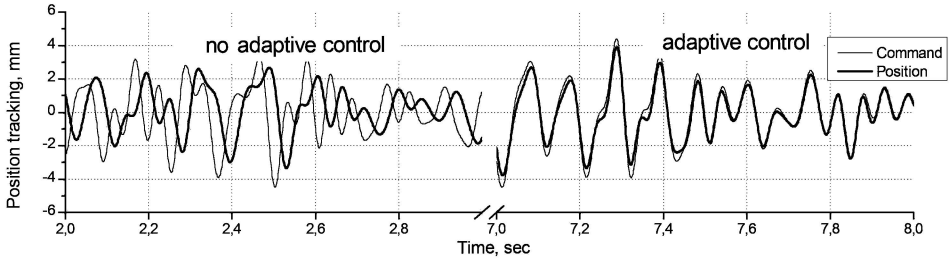

(a) Position tracking transient of adaptive controller

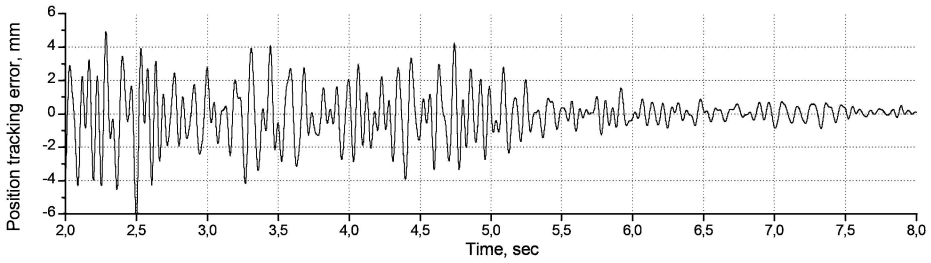

(b) Position tracking error

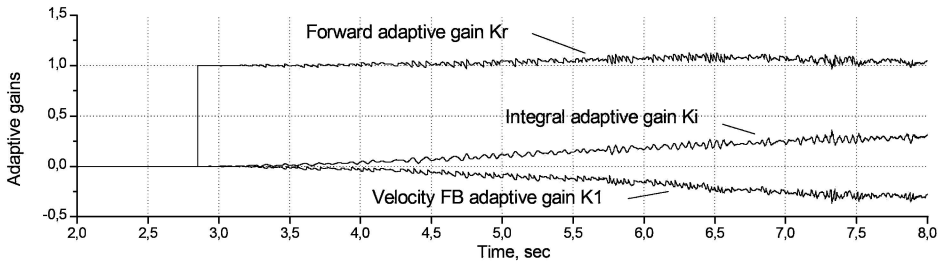

(c) Adaptive gains

Fig. 14 Transient response following transition from PIDL control to adaptive control

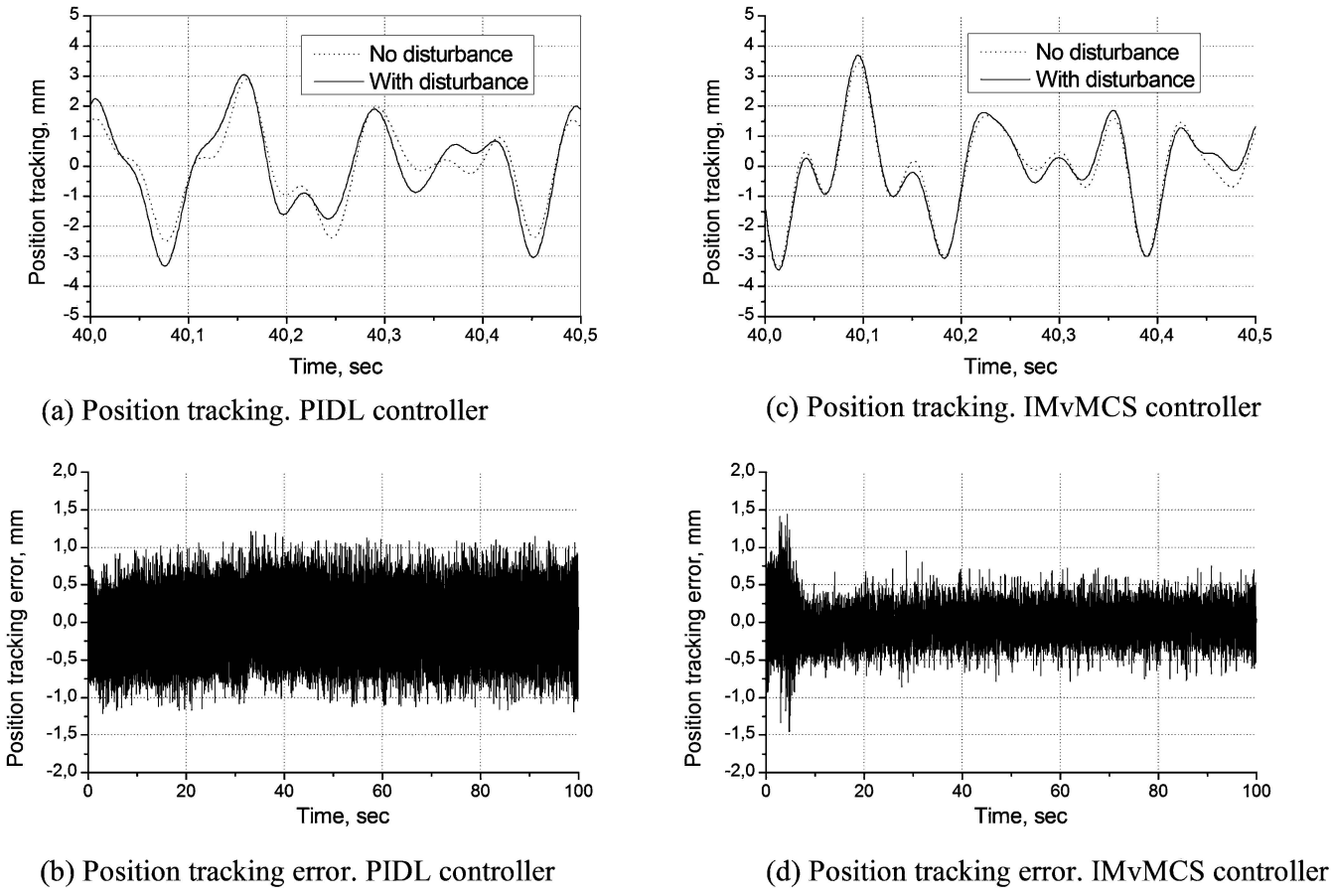

Fig. 15 Comparison of PIDL and adaptive controller

cases, for both control schemes, over a period of 100 s. It can be seen that the adaptive controller outperforms the PIDL controller by a factor of nearly two.

Disturbance rejection capabilities of the two fixed-gain inverse model controllers are compared with the adaptive controller performance in Fig. 16. The input was a filtered random signal with a 20 Hz bandwidth. The figure illustrates, on an enlarged time scale, the filtered trajectory tracking for all three controllers. Figures 17(a) to (c) show the position tracking error for operation without the disturbance. And finally Figs 17(d) to (f) depict position tracking error for the case when the disturbance is present. All controllers showed a degradation in position tracking accuracy in the presence of the disturbance. The 'case 1' scheme, with solely the inverse of the estimated plant transfer function being fed forward, showed the worst performance for both the disturbed and undisturbed cases. 'Case 2' showed better position tracking, while the adaptive controller achieved the best result. In order to summarize the overall performance, an integral square error (ISE) index was used to evaluate the magnitude of the tracking error over time for both the disturbed and undisturbed cases. The index was calculated by taking the integral of the square of position tracking error. The steepness of the slope of the graph is a measure of the accuracy of position tracking. The results are presented in Fig. 18. It can be seen that the adaptive controller has a shallower slope for both disturbed and undisturbed cases, when compared with other controllers, reflecting its superior performance.

During testing, adaptive gain drift was observed. This was encountered for low levels of excitation and for square-wave input signals. An optional solution to this problem is to use a gain bound modification of the adaptive controller, as proposed in reference [**16**].

5 CONCLUSIONS

An adaptive control scheme for multi-axis hydraulic test rigs has been developed and implemented on a MAST rig. The adaptive controller was designed on the basis of a velocity cascade combined with an inverse model feed-forward path. The aim was

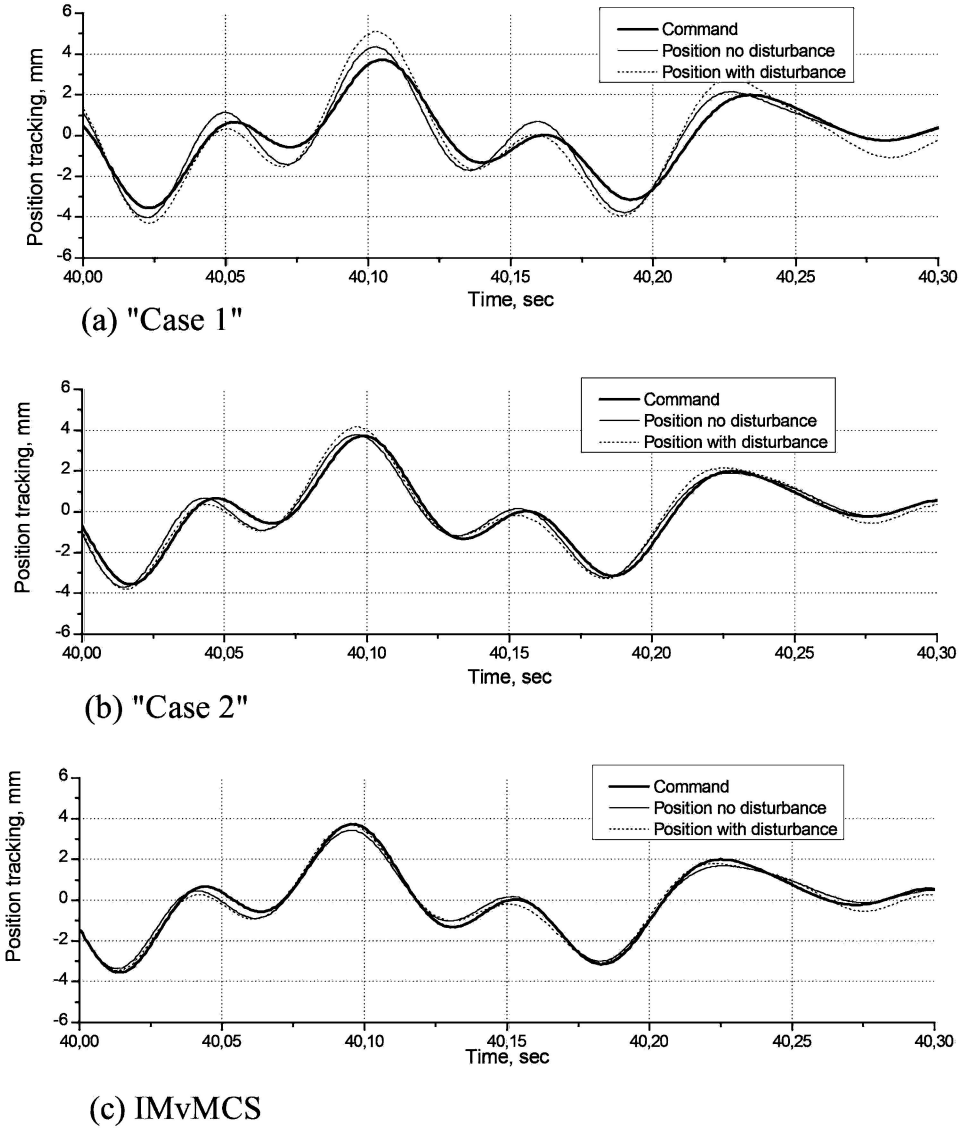

Fig. 16 Position tracking of controllers for disturbed and undisturbed cases

to minimize inter-axis interaction between the hydraulic actuators, and ensure acceptably good robust tracking of the command signal. Performance has been assessed through comparison with a fixed-gain PIDL scheme and with two fixed-gain inverse model schemes.

A number of practical issues were addressed during the implementation of the adaptive controller. The compliance of the cylinder mount resulted in errors when generating a velocity signal from the piston rod position and acceleration signals. This prompted the introduction of an additional acceleration measurement of the cylinder mount. Pressure ripple in the hydraulic circuit was found to introduce noise in the accelerometer signals and made it impractical to use acceleration feedback directly in the adaptive controller owing to stability issues. However, exclusion of the acceleration signal introduced a limitation on the bandwidth of the tracking capability of the adaptive controller to 15 Hz, and degraded the overall tracking performance. In addition, tests undertaken with a low level of command signal excitation and with a square-wave demand were found to result in gain drift. Thus, depending on the nature of the command signal, additional measures need to be undertaken: in the case of square-wave inputs, an inverse model filter with a lower bandwidth is required; and for single sine-wave inputs with low level excitation, a gain bound method may be applied.

Experimental testing has shown that the new adaptive control scheme outperformed a classical PIDL controller and two other fixed-gain controllers designed on the two-degrees-of-freedom controller principle. The adaptive controller has been

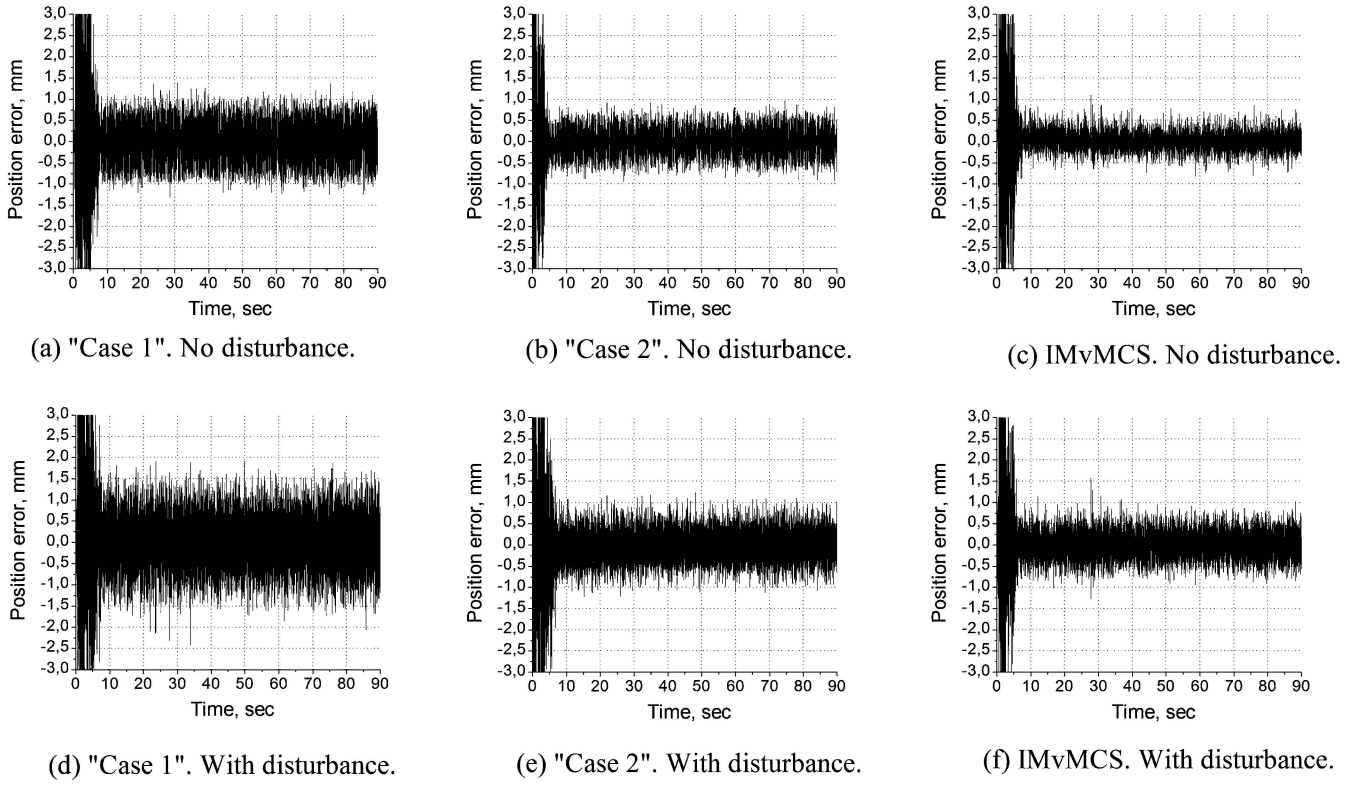

Fig. 17 Position tacking errors of controllers for disturbed and undisturbed cases

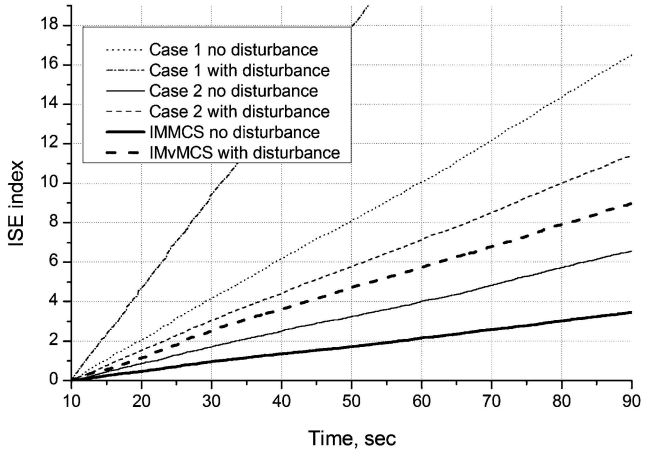

Fig. 18 Integral square error (ISE) index for different control schemes (random signal input)

demonstrated to be a potentially effective approach to control multi-axis hydraulic test rigs. It is intended that an analysis of the new algorithm will be published in the future. It should be noted that the new scheme has been assessed for the case where the disturbance has a specific frequency rather than a broadband excitation, which may occur in some applications. Further work needs to be undertaken to assess the ability of the controller to counteract broadband disturbances.

ACKNOWLEDGEMENTS

The authors wish to express thanks to Dr Andrew Plummer of Instron Structural Testing Systems (IST®) for his support and perceptive comments in relation to the work reported in the current paper. Grateful thanks are also extended to the University of Bath and Instron Structural Testing Systems (IST®) for a jointly funded studentship for Andrey Gizatullin.

REFERENCES

1 **Plummer, A. R.** Non-linear control of a flight simulation motion system. IEEE Conference on *Control applications*, 1994, Vol. 1, pp. 365–370.
2 **Tsukamoto, N.** and **Yokota, S.** Two-degree-of-freedom control with parallel feedforward compensators (the effects on the control of a six-link electro-hydraulic serial manipulator). 5th JFPS International Symposium on *Fluid power*, Nara, Japan, November 2002, Vol. 2, pp. 597–602.
3 **De Cuyper, J., Swevers, J., Verhaegen, M.,** and **Sas, P.** H_∞ feedback control for signal tracking on a 4 poster test rig in the automotive industry. International Conference on *Noise and vibration*, Leuven, Belgium, 13–15 September 2000, p.

4 **De Cuyper, J., Vaes, D., Dehandschutter, W., Swevers, J., Verhaegen, M.,** and **Sas, P.** Experimental H_∞ control to improve an industrial off-line tracking control scheme on an automotive suspension test rig. Conference on *Control applications*, IFAC, Glasgow, September 2002, p.

5 **Edge, K. A.** and **Gomes de Almeida, F.** Decentralized adaptive control of a directly driven hydraulic manipulator. Part 1: theory; Part 2: experiment. *Proc. Instn Mech. Engrs, Part I: J. System and Control Engineering*, 1995, **209**, 191–205.

6 **Gomez, E. G.** *Application of the MCS algorithm to the control system of the Bristol Shaking Table*. PhD thesis. Faculty of Engineering, University of Bristol, Bristol, 1999.

7 **Stoten, D. P.** Implementation of minimal control synthesis on a servo-hydraulic testing machine. *Proc. Instn Mech. Engrs, Part I: J. System and Control Engineering*, 1992, **206**, 189–194.

8 **Stoten, D. P.** and **Benchoubane, H.** Empirical studies of an MRAC algorithm with minimal controller synthesis. *Int. J. Control*, 1990, **51**(4), 823–849.

9 **Stoten, D. P.** and **Benchoubane, H.** Robustness of a minimal controller synthesis algorithm. *Int. J. Control*, 1990, **51**(4), 851–861.

10 **Stoten, D. P.** *The adaptive minimal control synthesis algorithm with integral action*, 1995, pp. 1646–1651 (IEEE, New York).

11 **Hessburg, T. M.** and **Kranz, D. G.** Feedforward control (based on model invertion) and system performance prediction using high-fidelity nonlinear dynamic system modelling. In Proceedings of the 1997 IEEE International Conference on *Control applications*, Hartford, CT, USA, 1997, pp. 57–62.

12 **Bitmead, R. R.** Persistence of excitation conditions and the convergence of adaptive schemes. *IEEE Trans. Inf. Theory*, 1984, **IT-30**(2), 183–191.

13 **Mareels, M. Y. I.** and **Bitmead, R. R.** Bifurcation effects in robust adaptive control. *IEEE Trans. Circuits and Systems*, 1988, **35**(7), 835–841.

14 **Stoten, D. P.** Fusion of kinetic data using composite filters. *Proc. Instn Mech. Engrs, Part I: J. System and Control Engineering*, 2001, **215**, 483–497.

15 **Rey, G. J., Bitmead, R. R.,** and **Johnson, C. R. Jr** The dynamics of bursting in simple adaptive feedback systems with leakage. *IEEE Trans. Circuits and Systems*, 1991, **38**(5), 476–488.

16 **Stoten, D. P.** and **Sebusang, S. E. M.** Gain bounds in the minimal controller synthesis algorithm. *Proc. Instn Mech. Engrs, Part I: J. System and Control Engineering*, 1998, **212**(1), 345–359.

APPENDIX

Notation

A	effective piston area
B	bulk modulus
$\boldsymbol{C}_e$	compensation vector
IMvMCS	inverse model velocity minimal control synthesis
ISE	integral square error (index)
$\boldsymbol{K}$	adaptive feedback gains vector
K_i	integral adaptive gain
K_1	velocity feedback adaptive gain
K_2	acceleration feedback adaptive gain
K_{M}	normalized adaptive controller model gain
K_{M1}	model gain for comparative controller 'case 1'
K_{M2}	model gain for comparative controller 'case 2'
K_{P}	plant gain
$\tilde{K}_{\mathrm{P}}$	plant gain estimate
K_{QP}	valve flow-pressure coefficient
K_{QX}	valve flow-spool displacement coefficient
K_{R}	forward adaptive gain
K_{V}	flow gain
MAST	multi-axis shaking table
MCS	minimal control synthesis
MCSIA	MCS controller with integral action
MRAC	model reference adaptive controller
M	mass of the load
PID	proportional + integral + derivative (controller)
PIDL	proportional + integral + derivative + lag (controller)
p_1, p_2	pressures in actuator chambers
p_{L}	load pressure
p_{LO}	load pressure linearization value
p_{R}	return line pressure
p_{S}	supply line pressure
p_{SYS}	system pressure
$\Delta P_{\mathrm{Rated}}$	rated pressure drop across the valve
Q	flowrate
Q_{Rated}	rated flowrate
r	reference command signal
s	Laplace operator
u	servo-valve command signal, control signal
vMCS	velocity minimal control synthesis
V_{o}	trapped volume in the cylinder chambers
$W_{\mathrm{HA}}(s)$	linearized actuator transfer function
x	piston rod position
$\boldsymbol{x}$	plant states vector
$\dot{x}$	piston rod velocity
$\ddot{x}$	piston rod acceleration
$\boldsymbol{x}_e$	error states vector
$\dot{x}_e$	velocity error

x_i	integral state error
$\boldsymbol{x}_{\mathrm{M}}$	model states vector
$\dot{x}_{\mathrm{M}}$	model velocity
x_{SV}	servo-valve spool position
x_{SVO}	servo-valve spool position linearization value
α	integral adaptive weight
β	proportional adaptive weight
ξ_{M}	adaptive controller model damping ratio
ξ_{M1}	model damping ratio for comparative controller 'case 1'
ξ_{M2}	model damping ratio for comparative controller 'case 2'
ξ_{P}	plant damping ratio
$\tilde{\xi}_{\mathrm{P}}$	plant damping ratio estimate
ω_{FILT}	filter natural frequency
ω_{M}	adaptive controller model natural frequency
ω_{M1}	model natural frequency for comparative controller 'case 1'
ω_{M2}	model natural frequency for comparative controller 'case 2'
ω_{P}	plant natural frequency
$\tilde{\omega}_{\mathrm{P}}$	plant natural frequency estimate